Available online at www.sciencedirect.com
ScienceDirect
Journal of Power Sources 174 (2007) 421–427
JOURNAL OF POWER SOURCES
www.elsevier.com/locate/jpowsour

Structural evolution of ramsdellite-type $Li_xTi_2O_4$ upon electrochemical lithium insertion–deinsertion ($0 \leq x \leq 2$)

A. Kuhn [a,*], C. Baehtz [b], F. García-Alvarado [a]

[a] *Departamento de Química, Universidad San Pablo-CEU, E-28668 Boadilla del Monte, Madrid, Spain*
[b] *Institute of Materials Science, University of Technology Darmstadt, D-64287 Darmstadt, Germany*

Available online 28 June 2007

Abstract

Structural evolution during topotactical electrochemical lithium insertion and deinsertion reactions in ramsdellite-like $Li_xTi_2O_4$ has been followed by means of *in situ* X-ray diffraction techniques. The starting $Li_xTi_2O_4$ ($x = 1$) exists as a single phase with variable composition which extends in the range $0.50 \leq x \leq 1.33$. However, beyond the lower and upper compositional limits, two other single phases, with ramsdellite-like structure, are detected. The composition of these single phases are: TiO_2 upon lithium deinsertion and $Li_2Ti_2O_4$ upon lithium insertion. Both TiO_2 and $Li_2Ti_2O_4$ are characterized by narrow compositional ranges. The close structural relationship between pristine $LiTi_2O_4$ and the inserted and deinserted compounds together with the relative small volume change over the whole insertion–deinsertion range (not more than 1.1% upon reduction) is a guaranty for the high capacity retention after long cycling in lithium batteries. The small changes in cell parameters well reflect the remarkable flexibility of the ramsdellite framework against lithiation and delithiation reactions.

Keywords: Ramsdellite $LiTi_2O_4$; Lithium titanate; Electrochemical lithium insertion and deinsertion; *In situ* X-ray diffraction; *In situ* synchrotron radiation

1. Introduction

Lithium titanates, which are known in spinel and ramsdellite form, are interesting candidates as negative electrodes in rechargeable lithium batteries. Presently, they are being evaluated for use in the next generation of secondary lithium cells. The most widely considered metal oxide for low potential applications is spinel $Li_4Ti_5O_{12}$, reported as a zero-strain insertion compound [1–3]. Indeed, it is used as a commercial negative electrode [4–6]. Similar performances have been reported for the spinel $LiTi_2O_4$, and a computational study of the electrochemical Li insertion reaction has been recently published [7]. The high temperature form of $LiTi_2O_4$ exhibits the ramsdellite type structure and has been first described by Petrov and Tsolovski [8]. Irvine's group followed in detail the spinel to ramsdellite transition by means of high temperature neutron diffractometry [9]. Akimoto et al. showed that all lithium can be chemically removed from single crystals of $LiTi_2O_4$ to yield the ramsdellite form of TiO_2 [10]. Several reports on the electrochemical Li insertion has been published regarding the electrochemical performances as electrode material [11,12].

First reported for the γ-polymorph of manganese dioxide [13], the ramsdellite structure is composed of distorted edge-linked MO_6 octahedra pairs, which form infinite columns by sharing opposite edges. The resulting columns share corners to give an open framework structure. Attending to its unit cell, $LiTi_2O_4$ can be written as $(Li_2)_c[(Ti_4)_f]O_8$ [14], where c and f stand for channel and framework site, respectively. For $LiTi_2O_4$, one tetrahedral channel site, named T_1 site, left by the $[MO_6]$ skeleton framework is occupied by the Li^+ ions.

The main question concerning the intercalation mechanism into $LiTi_2O_4$, however, has not yet been answered. The flat potential behavior of TiO_2 with ramsdellite structure has been suggested to involve two two-phase equilibriums corresponding to compositions TiO_2–$LiTi_2O_4$ and $Li_1Ti_2O_4$–$Li_2Ti_2O_4$ [11]. Our previous electrochemical characterization [12] lead to the same conclusions, although further studies regarding the reaction mechanism have not yet been reported. The aim of the present work was then to investigate the structural changes that occur during the insertion and deinsertion of lithium in $LiTi_2O_4$. For this purpose, the structural evolution in ramsdellite-type $LiTi_2O_4$ upon Li insertion–deinsertion reactions has been monitored *in situ* by use of conventional X-rays. In addition, a more detailed study has been performed *in situ* in an operating cell by use of synchrotron radiation, which provides higher resolution.

* Corresponding author. Tel.: +34 91 372 47 35; fax: +34 91 351 04 75.
E-mail address: akuhn@ceu.es (A. Kuhn).

0378-7753/$ – see front matter © 2007 Elsevier B.V. All rights reserved.
doi:10.1016/j.jpowsour.2007.06.147

2. Experimental

2.1. Synthesis of positive electrode material $LiTi_2O_4$

$LiTi_2O_4$ has been prepared in powder form as previously reported [9]. The synthesis route included Li_2TiO_3, TiO_2 and Ti metal:

$$2Li_2TiO_3 + 5TiO_2 + Ti \rightarrow 4LiTi_2O_4$$

The following high-purity reagents were used, Li_2CO_3 (Aldrich), Ti metal (Johnson Matthey) and TiO_2 anatase (Aldrich). Li_2TiO_3 itself has been obtained by reaction of Li_2CO_3 with TiO_2 at 800 °C. The ramsdellite was prepared using Li_2TiO_3, TiO_2 and Ti metal in the appropriate ratios. The reactants were mixed under acetone and then pressed to 13 mm diameter pellets. The pellets were transferred to a copper container which was placed in a quartz ampoule, sealed under vacuum and heated at 1000 °C for 72 h. At the end of the heating period, the sample was rapidly cooled to room temperature by quenching in an ice-water bath.

2.2. Electrochemical lithium insertion

Positive electrodes for the electrochemical lithium insertion studies were prepared as 8 mm diameter pellets consisting of active material, carbon black (Super-S) and Kynarflex (Elf-Atochem) as a binder in the weight ratios 85:10:5. Metallic lithium (Aldrich) was used as both negative and reference electrode. A circular glass fiber disk was used as separator, previously soaked in the electrolyte, which consisted of a 1 M solution of $LiPF_6$ in 2:1 EC + DMC (LP31, Selektipur®, Merck). Swagelok™-type cells were assembled with the aforementioned components in an argon-filled glove box (Vac-System, $H_2O < 1$ ppm) and then discharged and charged by use of a MacPileII multichannel system (Bio-Logic, France) in galvanostatic mode applying a typical current density of 0.10 mA cm^{-2} (C/20 rate).

2.3. In situ experiments

In situ experiments using conventional X-ray diffraction (XRD) were carried out on a STOE diffractometer working in reflection mode. Monochromatic radiation (Cu $K\alpha_1$; $\lambda = 1.5406$ Å) was used. Diffraction patterns were recorded in the selected 2θ-range 15–55°. Data collection for each pattern was about 36 min. A mixture of $LiTi_2O_4$, carbon black and binder (79:16:5 weight ratio) conformed to 13 mm diameter pellets was the positive electrode. The amount of active material $LiTi_2O_4$ was about 30 mg in each pellet. The *in situ* cell was assembled in an argon filled glove box and connected to a MacPile multichannel controller, on which data were collected in galvanostatic mode. Before the initiation of discharge and charge experiments, a pattern of the starting compound, $LiTi_2O_4$, was collected. A complete discharge–charge cycle was performed in galvanostatic mode (constant current density of 0.18 mA cm^{-2}). The lower cut-off voltage was here limited to 0.9 V. Under these conditions, the intercalation of one Li ion per formula unit was completed in 23 h. Once the intercalation of one Li ion had been achieved, the cell was recharged to the starting rest potential. On the other hand, a complete cycle, but started on charge was performed under identical experimental conditions.

In situ synchrotron X-ray diffraction (SXRD) experiments were performed at the *B*2 line at HASYLAB [15], working in transmission mode using a circular *in situ* XRD cell that has been previously described [16]. Radiation of wavelength was 0.709564 Å. A scintillation counter with an analyzing crystal, in front of it for high resolution, was used as the detector. As a positive electrode, a mixture of $LiTi_2O_4$, carbon black and binder was used and directly deposited as 13 mm diameter pellet in the *in situ* cell of the SXRD machine. For the SXRD experiments, a MPG multichannel controller has been used. Prior to the charge and discharge experiments, a pattern of the starting compound, $LiTi_2O_4$ was collected. In the first series of experiments, the cell was discharged in galvanostatic mode under a constant current density of 0.11 mA cm^{-2}, which allowed the intercalation of one Li ion per formula unit at C/12 rate. The lower cut-off voltage limit was 1.25 V. Once the intercalation had been finished, the cell was charged for deinsertion to a maximum potential of 3 V under the same galvanostatic conditions.

3. Results and discussion

3.1. Electrochemical lithium insertion

The electrochemical lithium insertion in $Li_xTi_2O_4$ ($x = 1$) has been reported [11,12]. Fig. 1a shows the complete voltage-composition (left axis) profile and the incremental capacity (right axis) curve of a Li/$LiTi_2O_4$ cell, previously full charged, in galvanostatical mode at a current density of 0.18 mA cm^{-2}. The incremental capacity curve is dominated by two main (reversible) peaks at 1.32 and 2.2 V, in agreement with earlier reports using cyclic voltammetry [12]. Additional, three smaller peaks are also observed in the intermediate range, 1.5–2.1 V, especially a peak arising at 2.15 V and separated from the main peak at 2.2 V by only ca. 50 mV. In the voltage-composition profile (Fig. 1a), several regions are distinguishable, indicative of different reductive processes during the deinsertion–insertion reaction. A complete discharge performed under slower experimental conditions is shown as a typical voltage-composition plot in Fig. 1b. The S-shaped voltage-composition curve at the beginning of the insertion and deinsertion reaction in $Li_1Ti_2O_4$ within the 2.1–1.5 V range points out that a solid solution is formed (labeled as II). Small peaks located at 1.6, 2.0 and 2.15 V can be detected in the incremental capacity curve. It has been reported that these three peaks may reflect the presence of several possible sites for Li insertion [11].

Additional, the flat potential curves observed when more lithium is inserted into and deinserted from $Li_1Ti_2O_4$ correspond to the main peaks observed in the incremental capacity curve. They are observed in Fig. 1a at 1.32 and 2.20 V, respectively. These flat behaviors has been suggested to involve two two-phase equilibria, $TiO_2/Li_1Ti_2O_4$ and $Li_1Ti_2O_4/Li_2Ti_2O_4$ [11,12]. Thus, the end of the phase transformations would be marked by (a) the fully inserted single-phase $Li_2Ti_2O_4$,

labeled as III and (b) the fully deinserted single-phase TiO_2 (or Ti_2O_4), labeled as I. The apparent compositional existence ranges for these single phases can be estimated from experimental results performed under slower conditions as follows: phase I: $0 \le x \le 0.1$, phase II: $0.6 \le x \le 1.2$ and phase III: $1.9 \le x \le 2.0$. It has to be noted that the determined apparent compositional ranges depend on the discharge and charge rate used. While the insertion of one Li ion per formula unit is achieved after discharge, the deinsertion of one Li ion per formula was not achieved after full charge. Even in experiments performed under quasi-equilibrium conditions it has not been possible to completely remove one lithium, which is reflected by a value of $x \neq 0$ at the fully charged state. The misfit of data with the theoretical one-electron-one-lithium count was suggested to be due to a diffusion constrained deinsertion behavior related to the particle size of the high-temperature-prepared ramsdellite $LiTi_2O_4$ [11]. This fact should be taken in mind when dealing with the structural characterization by SXRD and the compositional ranges determined from electrochemical data. Longer electrochemical experiments would be, evidently, necessary in order to get a more detailed compositional-structural insight.

3.2. Structural evolution upon lithium insertion–deinsertion in $Li_1Ti_2O_4$

From the electrochemical results shown in Fig. 1, the existence of single-phases $Li_xTi_2O_4$ is suggested for the approximate

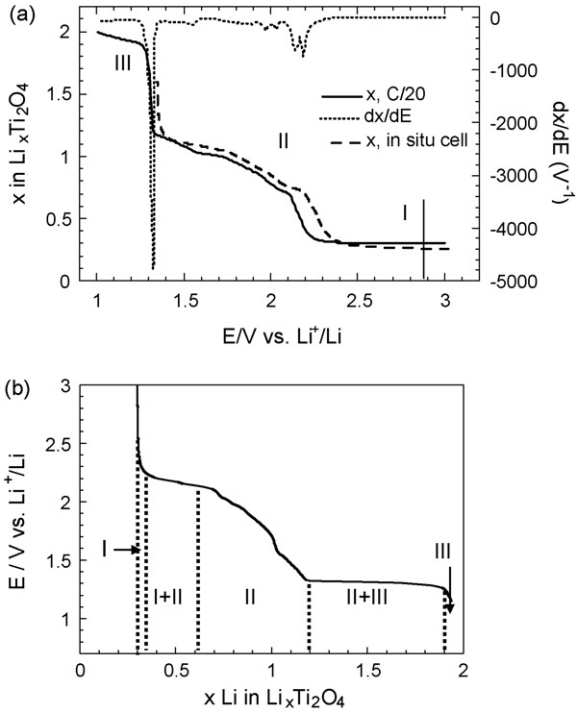

Fig. 1. (a) Voltage-composition curve (left hand, solid line) and the corresponding incremental capacity plot (right hand, dotted line) of a $Li_xTi_2O_4$/Li cell obtained in galavanostatic mode (C/20 rate). For comparison, the voltage-composition curve (dashed line) of the *in situ* cell used in the study with synchrotron radiation has been added. (b) Tentative phase diagram of $Li_xTi_2O_4$ ($0 \le x \le 2$) as a typical voltage-composition plot obtained in galvanostatic mode under ocv conditions.

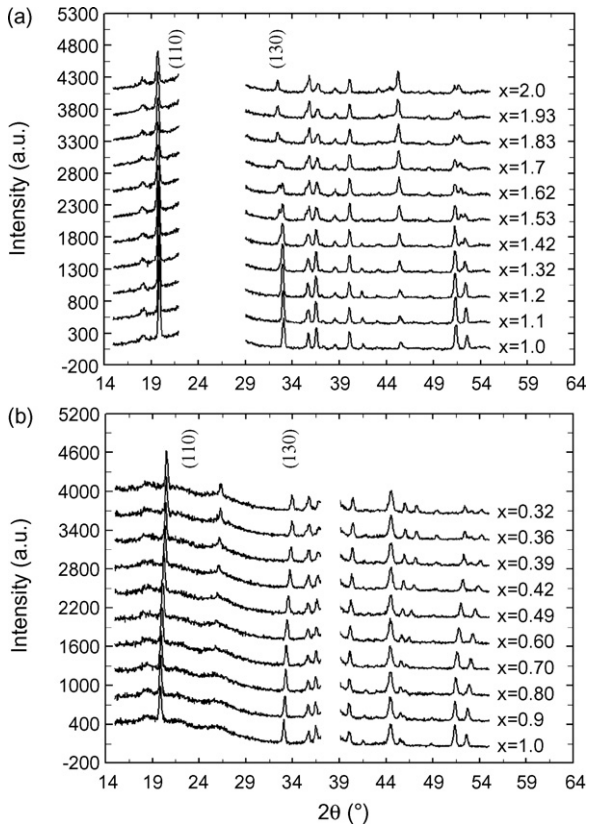

Fig. 2. Selected X-ray diffraction patterns measured under experimental *in situ* conditions with various Li composition x for $Li_xTi_2O_4$: $1.0 \le x \le 2.0$ (a) and $0.3 \le x \le 1.0$ (b).

compositional limits: $0 \le x \le 0.1$ (phase I), $0.6 \le x \le 1.2$ (phase II) and $1.9 \le x \le 2.0$ (phase III). The structural characterization of the $Li_xTi_2O_4$ system was initially performed by means of *in situ* powder technique using conventional X-ray diffraction. Fig. 2a shows a set of *in situ* X-ray diffraction patterns taken during the discharge of a Li/$LiTi_2O_4$ cell down to 1 V yielding the final composition $Li_xTi_2O_4$ with $x = 2$.

The evolution of reflections (1 1 0) and (1 3 0) as guides along the lithium insertion reaction will be highlighted here. Within the approximate compositional limit $1.0 \le x \le 1.32$, the continuous shift of both reflections to lower angles is characteristic of a solid solution domain, which was inferred from the electrochemical measurements (labeled as phase II). For $x > 1.32$, reflections get broad and asymmetric. Nevertheless, at higher x values, e.g. $x = 1.52$, the X-ray powder data clearly shows evidence for a second (lithium-inserted) phase (III) with emerging reflections at slightly lower angles. This is clearly observable for the (1 3 0) reflection. Finally, for x values greater than 1.9, no evidence of phase II in the diffraction patterns can be found, indicating that the phase transformation has been completed. In the range $1.9 \le x \le 2.0$, only a slight shift of reflections to lower angles is observed in this single phase III. Fig. 2b shows the *in situ* X-ray diffraction profiles obtained during the charge of a Li/$LiTi_2O_4$ cell. On charge, reflections (1 1 0) and (1 3 0) are shifted to higher angles, which underlines that phase II does exist for $x < 1$. For $x < 0.50$, broadening of reflections (1 1 0) and (1 3 0) is observed. However, the lithium-deinserted single

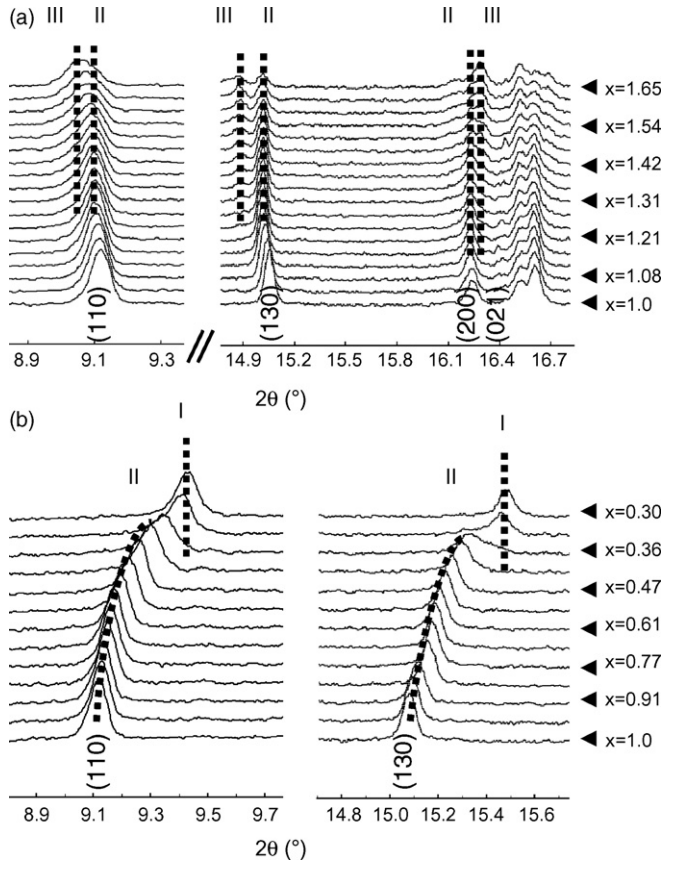

Fig. 3. Selected SXRD patterns of $Li_xTi_2O_4$ during discharge in the compositional range $1.0 \leq x \leq 1.65$ (a) and during charge in the compositional range $0.30 \leq x \leq 1.0$ (b).

phase (I), evidenced from the earlier electrochemical results, cannot be unambiguously confirmed in the X-ray powder patterns.

All these Li-driven structural changes in $Li_xTi_2O_4$ are much better observable in diffraction patterns obtained with SXRD, which are shown in Fig. 3a for the range including the reflections (1 1 0), (1 3 0), (2 0 0) and (0 2 1) along the discharge of a lithium cell in the range $1 \leq x \leq 1.65$. The observation of a single phase (II), two phases (II + III) and finally a single phase (III) during Li intercalation is in perfect agreement with electrochemical results earlier reported and pointed out in Fig. 1.

As it has been pointed out above, from the electrochemical results shown in Fig. 1, $Li_xTi_2O_4$ should exist as a single-phase solid solution with a rather wide compositional range ($1.32 \leq x \leq 0.45$), followed by a phase transformation for a higher degree of lithium deinsertion ($x < 0.45$). The phase released afterwards (labeled as I in Fig. 1) presents a narrow compositional existence range. Fig. 3b shows the evolution of reflections (1 1 0) and (1 3 0) in the SXRD patterns for the angular range taken during the charging of a $LiTi_2O_4$/Li cell. Phase II is the pristine compound, $LiTi_2O_4$. Upon lithium deinsertion, the continuous shift of both reflections to higher angles is characteristic of a solid solution domain within the compositional limits $1.0 < x < 0.47$. This was already assigned based on the electrochemical measurements (phase II).

Table 1
Unit cell parameters and reliability factors for the $Li_xTi_2O_4$ ramsdellite-type compounds (space group *Pbnm*)

	$x = 0$	$x = 1$	$x = 2$
a (Å)	4.8826(1)	5.0291(1)	5.0605(1)
b (Å)	9.4383(3)	9.6239(1)	9.7865(4)
c (Å)	2.96212(8)	2.9381(4)	2.9092(1)
R_p (%)	3.39	3.44	3.48
R_{wp} (%)	4.51	4.53	4.67
R_{exp} (%)	1.0	1.0	1.0
R_{Bragg} (%)	11.2	6.99	10.5

For $x < 0.45$, reflections get broad and asymmetric, revealing the coexistence of two ramsdellite-like phases that counteract. Upon charging, the reflections of the new phase I are growing at slightly higher 2θ values in comparison with the ones from the pristine compound. Nevertheless, at higher x values, e.g. $x = 0.30$, the X-ray powder data clearly demonstrate evidence for the new phase I with emerging reflections at slightly higher angles (clearly observable for the (1 3 0) reflection).

For quantitative analysis of the $Li_xTi_2O_4$ compounds, we employed the Rietveld method to determine the amount of each phase present along the lithium insertion–deinsertion. For fitting of the pristine $LiTi_2O_4$ phase (II) and the lithium-free TiO_2 (or Ti_2O_4) phase (I), we used the cell data given in the literature [9,10].

The structural parameters for the lithium-inserted phase $Li_2Ti_2O_4$ (labeled as III) were derived from the $LiTi_2O_4$ phase. The lattice parameters of the three phases are listed in Table 1, whereas the main structural parameters of the three $Li_xTi_2O_4$ phases ($x = 0$–2) as refined from synchrotron X-ray diffraction data are listed in Table 2.

As a general trend shortening of both a- and b-axis lengths with a slight growth of the c-axis is observed as the Li con-

Table 2
Atomic positional[a,b] (x–z) and isotropic thermal[c] (B) parameters for the $Li_xTi_2O_4$ ramsdellite-type compounds

Atom	x	y	z	B (Å^2)
Ti_2O_4 (TiO_2) ($x = 0$)				
Li	–	–	–	–
Ti	−0.0772(5)	0.1353(7)	1/4	1.1(4)
O1	0.636(2)	0.2602(9)	1/4	0.2(2)
O2	0.238(1)	−0.022(1)	1/4	0.2(2)
$LiTi_2O_4$ ($x = 1$)				
Li	−0.057	0.473	1/4	0
Ti	−0.0214(9)	0.1408(2)	1/4	1.3(4)
O1	0.694(2)	0.2762(9)	1/4	0
O2	0.242(1)	−0.030(1)	1/4	0
$Li_2Ti_2O_4$ ($x = 2$)				
Li	−0.057	0.473	1/4	0
Ti	−0.026(4)	0.139(1)	1/4	1.5(4)
O1	0.681(7)	0.261(3)	1/4	0
O2	0.249(4)	−0.022(3)	1/4	0

[a] All atoms in point positions 4c, $\pm(x, y, 1/4)$, $\pm(1/2 - x, 1/2 + y, 3/4)$.
[b] Lithium parameters have been fixed. Data were taken from ref. [11].
[c] B parameter was fixed to zero for those atoms, where refinement lead to negative values.

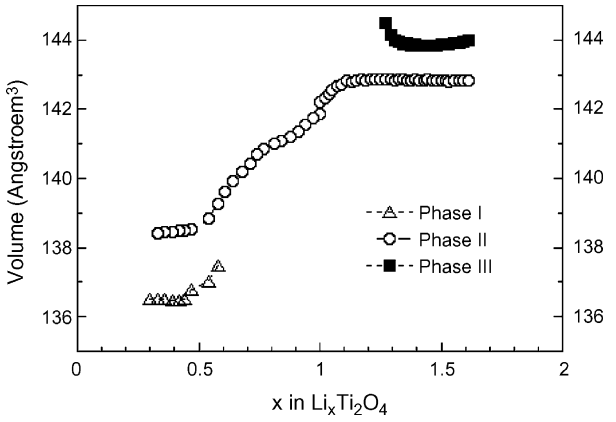

Fig. 4. Variation of the unit cell volume of the different phases present as a function of the nominal composition x in $Li_xTi_2O_4$.

tent decreases, which is in accordance with previous results from a single crystal study [10]. The orthorhombic unit cell with space group *Pbnm* expands isotropically during discharge (Table 1) of $LiTi_2O_4$. The lattice parameters in $Li_2Ti_2O_4$ reflect a 0.6% increase in a, a 1.7% in b and a 1.0% decrease in c, with respect to $LiTi_2O_4$, with an overall expansion of the unit cell of 0.9%. During the charge process, the expected inverse variation is observed. The lattice parameter in TiO_2 represent a 2.9% decrease in a, a 12.9% in b and a 0.8% increase in c, with respect to $LiTi_2O_4$. An overall contraction of the unit cell of 4.0% is observed. Fig. 4 shows the evolution of the unit cell volume of phases I–III as a function of the compositional parameter x.

The graphic result of the Rietveld fitting of selected patterns taken along the whole lithium compositional range is shown in Fig. 5. The observed and calculated patterns are shown together with their difference for the following compositions: $x = 1.0$ (a) (pristine phase II); $x = 1.65$ (b) (phase mixture II + III); $x = 0.33$ (c) (phase mixture I + II). In addition to the reflections from the ramsdellite-like phases, the strong reflections from the Al-plunger (cathode current collector) and the Li-anode can be identified. The composition $x = 1.0$ falls into the single phase II solid solution domain, whereas the data corresponding to $x = 1.65$ and $x = 0.33$ are fitted to two closely related ramsdellite-like phases, II + III and I + II, respectively.

The experimental set-up of the electrochemical *in situ* equipment used in the synchrotron radiation study did not allow us to fully discharge the cell, e.g. to $x = 1$. However, we have found a good agreement of the combined structural-compositional data obtained by means of synchrotron radiation with those obtained using conventional X-rays.

The evolution of the phase ratios has been analyzed by Rietveld refinements, and the derived number of phases and their relative amounts as a function of the nominal composition x are given in Fig. 6. Starting from the $x = 1$ member, $LiTi_2O_4$, the amount of phase II is decreasing continuously for $x > 1.32$ during discharge, while the phase III is formed counteracting. The region comprising $1.32 \leq x \leq 1.90$ is characterized by a complete and reversible phase transformation II → III with retention of the orthorhombic ramsdellite structure. The single-

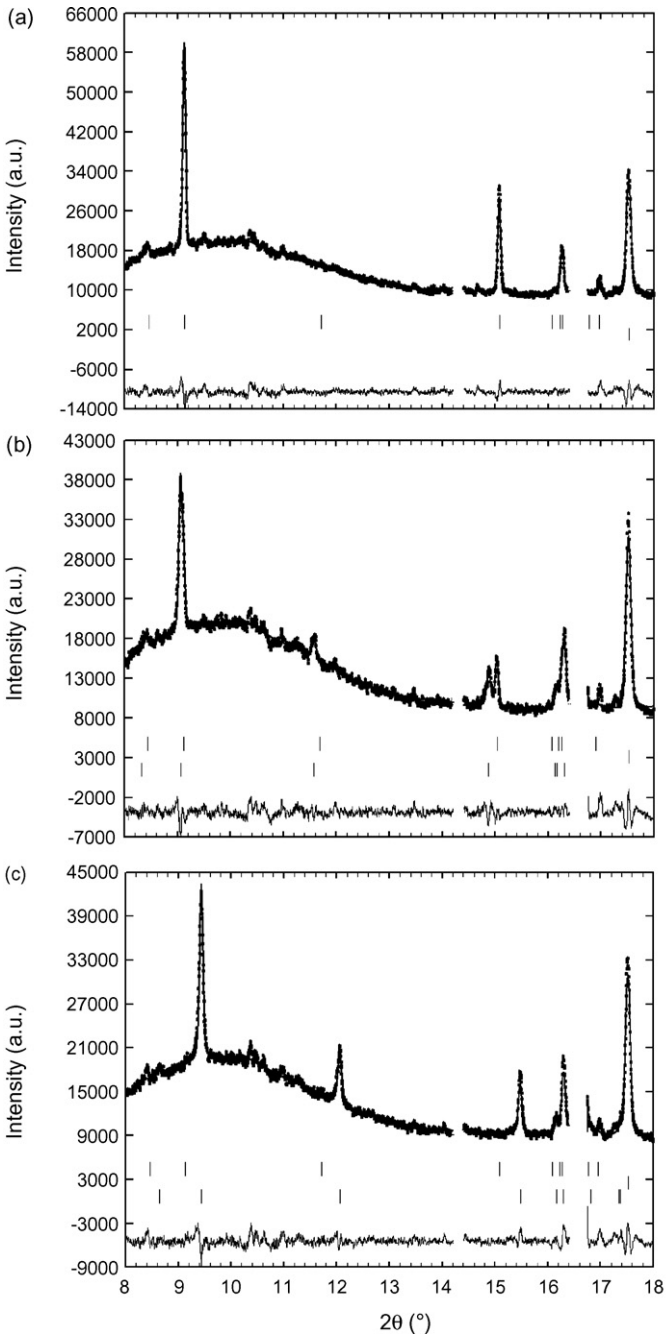

Fig. 5. Observed, calculated and difference of the fitting of SXRD data recorded for different compositions in the system $Li_xTi_2O_4$: $x = 1.0$ (pristine) (a), $x = 1.65$ (b) and $x = 0.33$ (c).

phase region for phase III is only narrow ($1.90 < x \leq 2.0$). On the other hand, phase II is maintained upon charge of $LiTi_2O_4$ up to $x = 0.60$. The region comprising $0.60 \leq x \leq 0.33$ is characterized by a complete and reversible phase transformation II → I with retention of the orthorhombic ramsdellite structure. The compositional existence range of phase I is very narrow ($0.30 \leq x \leq 0.33$).

It was not possible to accurately determine the positions of the Li^+ ions in the structures from the X-ray data, although further works are presently in progress. However, it can be seen that both lithium insertion into and deinsertion from the hexagonally

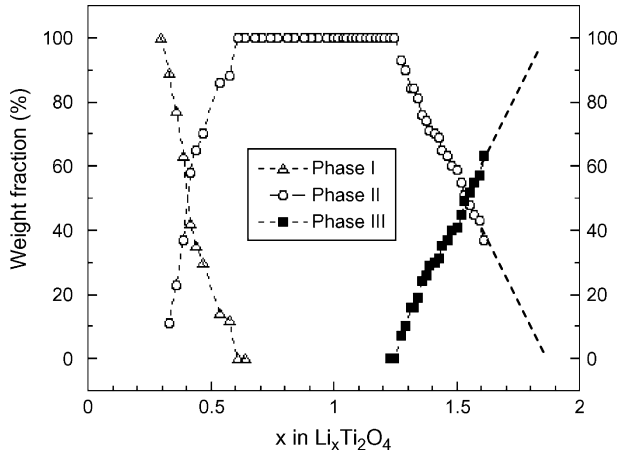

Fig. 6. Evolution of the number of phases and their relative weight fraction as a function of the nominal composition x in $Li_xTi_2O_4$.

close-packed array of $Li_1Ti_2O_4$ (Fig. 7b) causes a shear of the (2×1) ramsdellite blocks accompanied by a structural buckling, probably in response to the increasing electrostatic interaction between the lithium ions and the titanium ions in face-shared polyhedra. As a result of the shear the close-packed oxygen layers, which are initially parallel to the *bc* plane in $Li_1Ti_2O_4$ (indicated by dotted lines in Fig. 7b), are developed parallel to the *ac* plane in both lithiated and delithiated structures, $Li_2Ti_2O_4$ and TiO_2 (dotted lines in Fig. 7a and c, respectively).

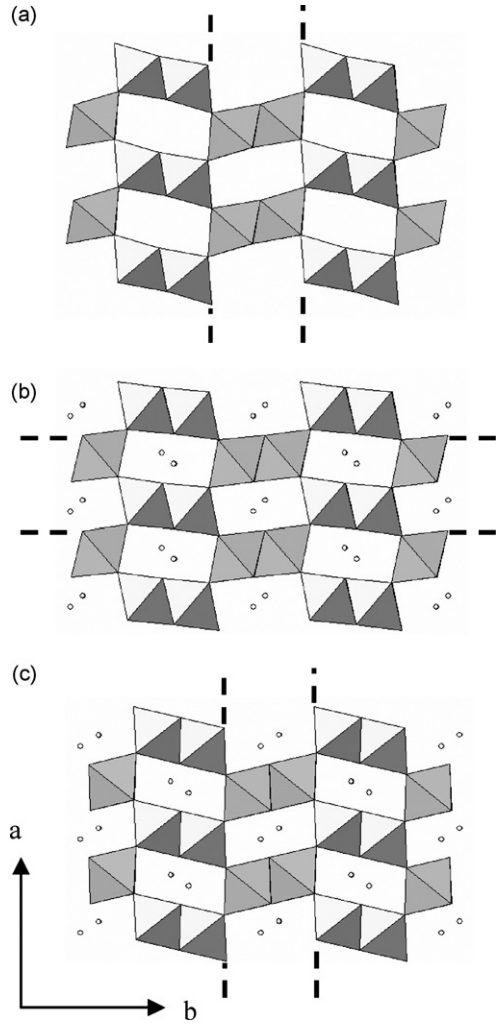

Fig. 7. The structures of (a) ramsdellite-TiO_2 and its lithiated products: (b) $LiTi_2O_4$ and (c) $Li_2Ti_2O_4$. Shaded octahedral contain $Ti^{4+/3+}$ ions, small open circle = Li^+ ions.

4. Conclusions

The different processes occurring during the electrochemical lithium insertion in $Li_xTi_2O_4$ have been successfully detected by using *in situ* X-ray diffraction methods. The structural characterization of ramsdellite-like $Li_xTi_2O_4$ in the range $0 \leq x \leq 2$ has shown that the basic structural framework is retained over the complete lithium compositional range. In situ diffraction analysis by means of high resolution synchrotron radiation allowed to distinguish between different ramsdellite-like phases with quite similar lattice constants along the lithium insertion–deinsertion reaction. Rietveld refinements of the SXRD patterns have shown that along the phase conversion the amount of each phase depends linearly on the amount of lithium. Upon discharge a very low change in the cell volume of $Li_xTi_2O_4$ is observed, which accounts for the excellent cycling properties of this material. Bearing in mind that the insertion reaction is developed at relative low voltage (ca. 1.4 V), the utility of $Li_xTi_2O_4$ as an anode in lithium ion batteries is hereby underlined. On the other hand, during the charge process of $Li_xTi_2O_4$ an intermediate deinsertion voltage is developed accompanied by a moderate volume change of 4.0%.

Acknowledgements

This work has been financially supported by the MEC (project MAT2004-03070-C05) and the Comunidad de Madrid (project S-0505/PPQ/0358). Authors thank Universidad San Pablo-CEU for financial and continuous support. This work was also supported by the European Community-Research Infrastructure Action through the Integrated Infrastructure Initiative "Integrating Activity on Synchrotron and Free Electron Laser Science"

References

[1] K.M. Colbow, J.R. Dahn, R.R. Haering, J. Power Sources 26 (1989) 397.
[2] E. Ferg, R.J. Gummov, A. De Kock, M.M. Thackeray, J. Electrochem. Soc. 141 (1994) L147.
[3] T. Ohzuku, A. Ueda, N. Yamamoto, J. Electrochem. Soc. 142 (1995) 1431.
[4] "Manganese Titanium Lithium Rechargeable", © 2005 Panasonic Corporation of North America, One Panasonic Way, Secaucus, NJ 07094, USA (www.panasonic.com/industrial/battery/oem/chem/lith/mangtit.htm).
[5] "Keramisches Anodenmaterial für 2.4V Lithium-Ionen Batterien", Süd-Chemie AG, 80333 München, Germany (www.sud-chemie.com/scmcms/web/content.jsp?nodeId=48578lang=de).
[6] L. Kavan, J. Procházka, T.M. Spitler, M. Kalbáč, M. Zukalová, T. Drezen, M. Grätzel, J. Electrochem. Soc. 150 (2003) A1000.
[7] W. Ra, M. Nakayama, Y. Uchimoto, M. Wakihara, J. Phys. Chem. B 109 (2005) 1130.
[8] K. Petrov, I. Tsolovski, Phys. Stat. Sol. A 58 (1980) K85.
[9] K.B. Richard, J. Gover, J.T.S. Irvine, A.A. Finch, J. Solid State Chem. 132 (1997) 382.

[10] J. Akimoto, Y. Gotoh, Y. Oosawa, N. Nonose, T. Kumagai, K. Aoki, H. Takei, J. Solid State Chem. 113 (1994) 27.
[11] R.K.B. Gover, J.R. Tolchard, H. Tukamoto, T. Murai, J.T.S. Irvine, J. Electrochem. Soc. 146 (1999) 4348.
[12] A. Kuhn, R. Amandi, F. García-Alvarado, J. Power Sources 92 (2001) 221.
[13] A.M. Byström, Acta Chem. Scand. 3 (1949) 163.
[14] J. Akimoto, Y. Gotoh, M. Sohma, K. Kawaguchi, Y. Oosawa, H. Takei, J. Solid State Chem. 110 (1994) 150.
[15] M. Knapp, C. Baehtz, H. Ehrenbergand, H. Fuess, J. Synchrotron Radiat. 11 (2004) 328.
[16] C. Baehtz, T. Buhrmester, N.N. Bramnik, K. Nikolowski, H. Ehrenberg, Solid State Ionics 176 (2005) 1647.